On the use of spatial modulation in aeronautical communications

Bilel Raddadi, Nathalie Thomas, Charly Poulliat, Marie-Laure Boucheret

On the use of spatial modulation in aeronautical communications

Bilel Raddadi, **Nathalie.Thomas**, **Charly Poulliat**, **Marie-Laure Boucheret**
University of Toulouse, INPT/ENSEEIHT, IRIT, France
{vorname.name}@enseeiht.fr

Abstract—In this work, we apply Spatial Modulation (SM) to in the so-called spectrally shaped SC-OFDM (SS SC-OFDM) at the transmitter. The idea behind SS SC-OFDM lies in applying a frequency window between the Fast Fourier Transform (FFT) and the Inverse Fast Fourier Transform (IFFT) in order to lower the side-lobes of the resulting time domain generated waveform. Thus, we can avoid the peak-to-average power ratio (PAPR) problem encountered in multicarrier systems. At the receiver, a reduced-rank (rr) Least Square (LS) channel estimation and a combining Minimum Mean Square Error (MMSE) equalization are used to retrieve the transmitted block of information bits, considering two flight scenarios for different environments.

I. INTRODUCTION

Nowadays, several studies are launched for the design of highly reliable and cost-effective communications systems that introduce Unmanned Aerial Vehicle (UAV) to monitor a very large civilian area [1].

The aircrafts can fly in a rich multipath environments. In this case, it is interesting to take advantage of using Multi-Input-Multi-Output (MIMO) techniques, since it exploit the decorrelation of received signals to improve detection at the receiver. In this context, we propose spatial modulation (SM) [2] [3] [4]. SM is relatively a new modulation technique for multi-antenna systems.

Considering N_t transmit antennas, differently from the classical modulation, SM modulation introduces a new dimension which is the index of the transmit antenna. Thus, the resulting index antenna indicates which transmit antenna is selected to sent the M-ary symbol in any given symbol duration T_s. In the following, we consider that a single antenna is selected to transmit the M-ary symbol. By using maximum power detection, the receiver will be able to detect, according to the Maximum Likelihood (ML) criterion, which one of the N_t antennas was selected to convey the considered M-ary symbol. The use of SM increases the overall spectral efficiency of the base-two-logarithm of the number of antennas.

High data rate communication system designs need for larger bandwidths, which, in turn, result in frequency selectivity of the wireless channel. In frequency selective channels, the presence of multipath components causes inter-symbol interference (ISI). To mitigate ISI by using a simple equalization at the receiver, we apply a multi-carrier modulation on each transmit antenna. In [2] [3] [4], Orthogonal Frequency Division Multiplexing (OFDM) is considered. However, high peak to average power ratio (PAPR) at the OFDM transmitter caused by the IFFT operation makes the design of amplifier

a challenging task. To address this issue, we consider, in this paper, the multi-carrier modulation SS SC-OFDM [5] [6] to avoid the peak-to-average power ratio (PAPR) problem encountered in in OFDM systems using spatial modulation.

This paper studies the application of the SM-MIMO technique using SS SC-OFDM in the case of aeronautical communications and especially the air to ground communications such as the mission link for UAV systems. According to the characteristics of the actual communication environment of aircraft, we study the downlink channel of aircraft data link and we derive a three dimensional channel model. Considering a possible Non-line-of-sight (NLOS) and a line-of-sight (LOS) mutipath channel between the aircraft and the ground base stations, a simulation of the performance in terms of Bit Error Rate (BER) is discussed.

The rest of this paper is organized as follows. Section II presents the system model, including SM modulation applied to SS SC-OFDM waveform as well as a description of receiver algorithms. The aeronautical channel case is studied in Section III by giving an associate three-dimensional channel model. Simulation results follow in Sections IV. Finally, Section V concludes this paper.

II. SYSTEM MODEL

The following notations are used throughout this paper. Bold and lowercase letters denote vectors, whereas bold and capital letters denote matrices. The notations $(.)^+,(.)^H$, and $(.)^T$ denote the pseudoinverse, Hermitian, and transpose of a vector or matrix, respectively, and $(.)^{-1}$ denotes the inverse of a matrix. $\lfloor (.) \rfloor$ stands for the integer part of $(.)$.

We consider a MIMO communications system with N_t transmit antennas and N_r receive antennas as shown in Fig.1.

A. Transmitter

Let us consider a binary sequence to be transmitted over a MIMO system. The transmitter groups this incoming bits into blocks of $\log_2(N_t \times M) \times K$ bits. The first $\log_2(N_t) \times K$ bits are mapped to select antenna vector $\mathbf{a} = [a_1, a_2, \ldots, a_K]$ containing the index in each symbol duration $a_k \in 1, \ldots, N_t$.

1) Space Allocation: The remaining $\log_2(M) \times K$ bits are mapped into a complex signal constellation vector $\mathbf{c} = [c_1, c_2, \ldots, c_K]$, where c_k ($c_k \in \{1, \ldots, M\}$) is selected from an M-ary complex signal constellation. From the vector $\mathbf{a}$, The modulated vector $\mathbf{c}$ is mapped to a $\mathbf{C} = [\mathbf{C}_1, \mathbf{C}_2, \ldots, \mathbf{C}_{N_t}]^T$
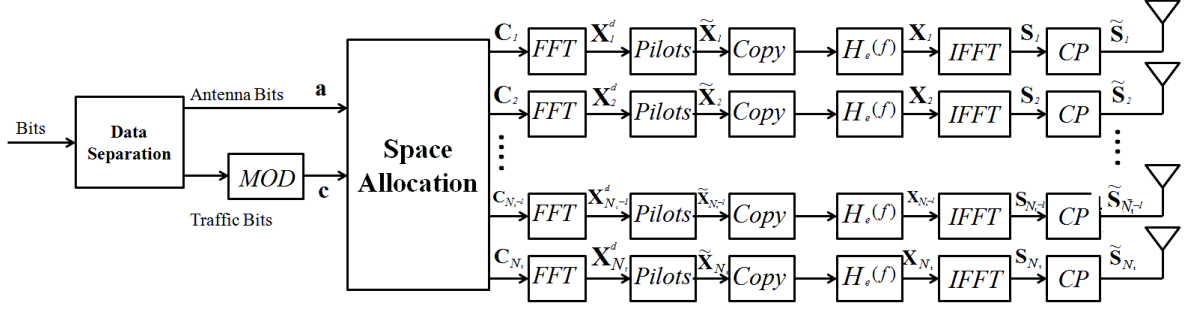
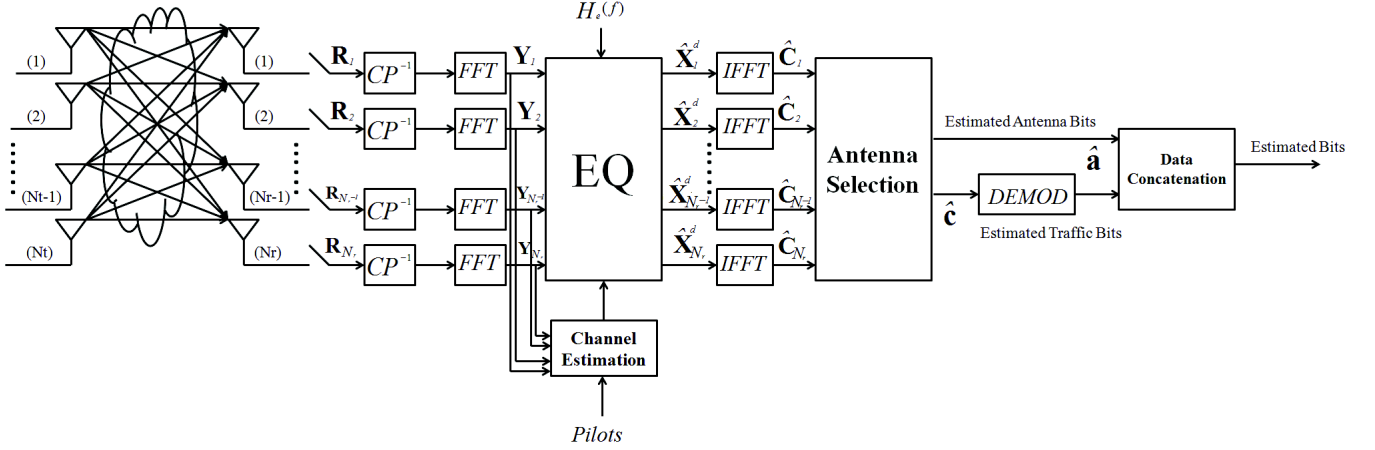Fig. 1. Spectrally Shaped SC-OFDM transmitter using Spatial modulation.

Fig. 2. Spectrally Shaped SC-OFDM receiver using Spatial modulation.

matrix having one nonzero element in each column at the position of the mapped transmit antenna number as follow:

$$\mathbf{C}_{n_t}(k) = \begin{cases} c_k, & \text{if } n_t = a_k. \\ 0, & \text{else.} \end{cases} \quad (1)$$

$$1 \le n_t \le N_t \qquad 1 \le k \le K$$

The Transmitter and the receiver of the proposed SM system model is shown in Fig.1 and Fig.2 respectively.

2) Frequency Domain: For each Transmit antenna n_t, The K incoming time domain symbols $\mathbf{C}_{n_t}$ are transformed to frequency domain by Fast Fourier Transform (FFT) to obtain a vector of K frequency symbols $\mathbf{X^d}_{n_t}$:

$$\mathbf{X^d}_{n_t}(k) = \sum_{m=0}^{K-1} \mathbf{C}_{n_t}(m) \ \exp(-2\pi j \frac{mk}{K}) \quad (2)$$

$$0 \le k \le K - 1$$

For Frequency channel estimation, we insert in each n_t antenna, a CAZAC (Constant Amplitude Zero Auto Correlation) sequence. The pilot symbols are allocated in order to have one nonzero element in each column at the position of index pilot insertion number (see Fig.3). All other elements in that column are set to zero to ensure the space orthogonality of the received pilot symbols. After pilot insertion we obtain:

$$\tilde{\mathbf{X}}_{n_t}(k) = \begin{cases} \mathbf{x_p}^{n_t}(\lfloor \frac{k}{\Delta} \rfloor), & \text{if } k \in I_{n_t}. \\ 0, & \text{if } k \in I_{n_t' \neq n_t}. \\ \mathbf{X^d}_{n_t}(k - \lfloor \frac{k}{\Delta} \rfloor), & \text{else.} \end{cases} \quad (3)$$

$$1 \le n_t \le N_t \qquad 1 \le k \le (K + N_p)$$

where, $\mathbf{x_p}^{n_t}$ is a vector of N_p CAZAC pilot symbols to be inserted into data sequence $\mathbf{X^d}_{n_t}(k)$ at the index frequency position $I_{n_t} = (I_{n_t}[1], I_{n_t}[2], \ldots, I_{n_t}[N_p])$. The pilot symbols are uniformly inserted into the data sequence with a spacing Δ.

As shown in Fig.1, the obtained $\tilde{\mathbf{X}}_{n_t}$ is extended to $\mathbf{X}_{n_t}$ of $N = K + N_p + 2.T_{cp} = (1 + \beta)(K + N_p)$ frequency symbols by addition of a $T_{cp} = \frac{\beta}{2}(K + N_p)$ cyclic prefix and also a T_{cp} cyclic suffix at the begin and the end respectively, resulting a cyclic extension.

The $\mathbf{X}_{n_t}$ sequence is multiplied by the sampled frequency response of a shaping filter $\underline{H}_e(n)$ before an Inverse Fast
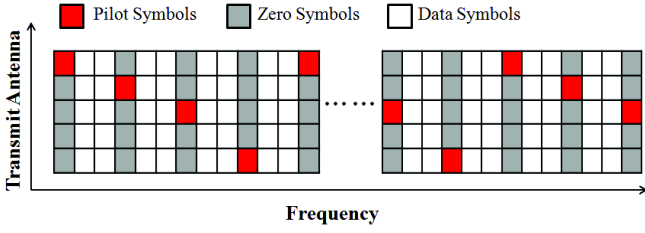
Fig. 3. Frequency data and pilots Allocation.

Fourier Transform (IFFT) transformation to have a time domain sequence $\mathbf{S}_{n_t}$ of N symbols.

$$\mathbf{S}_{n_t}(n) = \sum_{m=0}^{N-1} \mathbf{X}_{n_t}(m).\underline{H}_e(m) \, \exp(2\pi j \frac{mn}{N}) \quad (4)$$

$$0 \le n \le N-1$$

The expansion of the transmission bandwidth results from the choice of frequency domain shaping filter $\underline{H}_e(n)$. In this paper, we assume having a Root Raised Cosine (RRC) pre-shaping filter with a roll-off β given by:

$$\underline{H}_e(n) = \begin{cases} \sqrt{\cos(\frac{\pi}{2}(1 - (\frac{1+\beta}{\beta})\frac{n}{N}))}, & \text{if } 0 \le n \le \frac{\beta N}{1+\beta}. \\ 1, & \text{if } \frac{\beta N}{1+\beta} < n < \frac{N}{1+\beta}. \\ \sqrt{\cos(\frac{\pi}{2}(-\frac{1}{\beta} + (\frac{1+\beta}{\beta})\frac{n}{N}))}, & \text{if } \frac{N}{1+\beta} \le n < N. \end{cases}$$

$$(5)$$

Thus, $N - (K + N_p) = \beta(K + N_p)$ extra sub-carriers are required, and the spectral efficiency of the system is reduced $\frac{1}{1+\beta}$ times. Some extra sub-carriers with low amplitude can lead to a lower PAPR of the output signal after IFFT. It is noted that performing a direct mapping of the FFT output to the IFFT central inputs without spectral pre-shaping is equivalent to using an RRC filter with a roll-off factor set to zero (regular SC-OFDM waveform).

Just after the IFFT operation, a Cyclic Prefix (CP) of length T_g samples is inserted at the beginning of each resulting vector $\mathbf{S}_{n_t}$ to obtain a $\tilde{\mathbf{S}}_{n_t}$ vector of $(N + T_g)$ SS SC-OFDM symbols, in order to cope with inter-symbol interference from the channel and maintain sub-carrier orthogonality.

The $\tilde{\mathbf{S}}$ matrix of $N_t \times (N + T_g)$ symbols to be transmitted from the N_t transmit antennas over the MIMO channel, $\mathbf{h}$, can be written as the following:

$$\tilde{\mathbf{S}} = [\tilde{\mathbf{S}}_1, \tilde{\mathbf{S}}_2, \dots, \tilde{\mathbf{S}}_{N_t}]^T \quad (6)$$

B. Discret equivalent MIMO channel impulse

The discret equivalent MIMO channel matrix $\mathbf{h}$ is a block matrix containing a set of $N_r \times N_t$ vectors each of length L ($T_g \ge L$). Each vector corresponds to the multipath channel gains between each transmit and receive antenna as follows:

$$\mathbf{h} = \begin{bmatrix} \mathbf{h}_{1,1} & \mathbf{h}_{1,2} & \dots & \mathbf{h}_{1,N_t} \\ \mathbf{h}_{2,1} & \mathbf{h}_{2,2} & \dots & \mathbf{h}_{2,N_t} \\ \vdots & \vdots & \ddots & \vdots \\ \mathbf{h}_{N_r,1} & \mathbf{h}_{N_r,2} & \dots & \mathbf{h}_{N_r,N_t} \end{bmatrix} \quad (7)$$

$\mathbf{h}_{n_r,n_t}$ is a size $L \times 1$ channel vector between receive antenna n_r and transmit antenna n_t containing all the multipath channel gains and can be written as follows:

$$\mathbf{h}_{n_r,n_t} = [\mathbf{h}_{n_r,n_t}(0), \mathbf{h}_{n_r,n_t}(1), \dots, \mathbf{h}_{n_r,n_t}(L-1)]^T \quad (8)$$

C. Receiver

After sampling, the received matrix $\mathbf{R} = \tilde{\mathbf{S}} \otimes \mathbf{h} + \mathbf{B}$, where $\mathbf{B}$ is the additive white Gaussian noise matrix and by abuse of notation $\otimes$ denotes time kronecker convolution.

1) Frequency Domain: After removing CP, the rows of the received matrix $\mathbf{R}$ are transformed to the frequency domain by using N_r FFT transformations. The resulting output is a matrix $\mathbf{Y} = [\mathbf{Y}_1, \mathbf{Y}_2, \dots, \mathbf{Y}_{N-1}]^T$ of size $N_r \times N$, which corresponds to the received data in the N frequency subchannels from the N_r receive antennas. Each column can be written as follows:

$$\begin{bmatrix} \mathbf{Y}_1(k) \\ \mathbf{Y}_2(k) \\ \vdots \\ \mathbf{Y}_{N_r}(k) \end{bmatrix} = \mathbf{H}(k) \begin{bmatrix} \mathbf{X}_1(k) \\ \mathbf{X}_2(k) \\ \vdots \\ \mathbf{X}_{N_t}(k) \end{bmatrix} + \begin{bmatrix} b_1 \\ b_2 \\ \vdots \\ b_{N_t} \end{bmatrix} \quad 0 \le k \le N-1$$

$$(9)$$

where $[b_1, b_2, \dots, b_{N_t}]^T$ is an additive white Gaussian noise vector and $\mathbf{H}(k)$ is the $N_r \times N_t$ discrete time-invariant frequency response channel matrix at the index frequency k:

$$\mathbf{H}(k) = \begin{bmatrix} H_{1,1}(k) & H_{1,2}(k) & \dots & H_{1,N_t}(k) \\ H_{2,1}(k) & H_{2,2}(k) & \dots & H_{2,N_t}(k) \\ \vdots & \vdots & \ddots & \vdots \\ H_{N_r,1}(k) & H_{N_r,2}(k) & \dots & H_{N_r,N_t}(k) \end{bmatrix} \quad (10)$$

$\mathbf{H}_{n_r,n_t}$ is a size $N \times 1$ frequency channel response vector between receive antenna n_r and transmit antenna n_t verifying:

$$\mathbf{H}_{n_r,n_t}(k) = \underline{H}_e(k) \sum_{l=0}^{L-1} \mathbf{h}_{n_r,n_t}(l) \, \exp(-2\pi j \frac{lk}{N}) \quad (11)$$

$$0 \le k \le N-1$$

2) Reduced-rank (rr) LS Channel Estimation: To estimate the frequency response of the MIMO channel, we extract from $\mathbf{Y}$ the useful symbols by removing the first T_{cp} columns and also the last T_{cp} columns to obtain an useful data matrix $\tilde{\mathbf{Y}} = [\mathbf{Y}(T_{cp}), \mathbf{Y}(T_{cp}+1), \dots, \mathbf{Y}((N - .T_{cp}) - 1)]$, where each column can be written as follows:

$$\tilde{\mathbf{Y}}(k) = \begin{bmatrix} \tilde{\mathbf{Y}}_1(k) \\ \tilde{\mathbf{Y}}_2(k) \\ \vdots \\ \tilde{\mathbf{Y}}_{N_r}(k) \end{bmatrix} = \tilde{\mathbf{H}}(k) \begin{bmatrix} \tilde{\mathbf{X}}_1(k) \\ \tilde{\mathbf{X}}_2(k) \\ \vdots \\ \tilde{\mathbf{X}}_{N_t}(k) \end{bmatrix} + \begin{bmatrix} b_1 \\ b_2 \\ \vdots \\ b_{N_r} \end{bmatrix} \quad (12)$$

$$\tilde{\mathbf{H}}(k) = \mathbf{H}(k + T_{cp}) \quad 0 \le k \le (N - 2.T_{cp}) - 1$$

After that, we extract from $\tilde{\mathbf{Y}}_{n_r}$ the sampled received signal, the sequence corresponding to pilot symbols. Thus we can write the resulting symbols to this matrix form:

$$
\begin{bmatrix}
\tilde{\mathbf{Y}}_{n_r}(I_{n_t}[1]) \\
\tilde{\mathbf{Y}}_{n_r}(I_{n_t}[2]) \\
\vdots \\
\tilde{\mathbf{Y}}_{n_r}(I_{n_t}[N_p])
\end{bmatrix}
= \mathrm{diag}(\mathbf{x}_p^{(n_t)})
\begin{bmatrix}
\tilde{\mathbf{H}}_{n_r,n_t}(I_{n_t}[1]) \\
\tilde{\mathbf{H}}_{n_r,n_t}(I_{n_t}[2]) \\
\vdots \\
\tilde{\mathbf{H}}_{n_r,n_t}(I_{n_t}[N_p])
\end{bmatrix}
+
\begin{bmatrix}
b_1 \\
b_2 \\
\vdots \\
b_{N_p}
\end{bmatrix}
\tag{13}
$$

Where, $[b_1, b_2, \ldots, b_{N_p}]^T$ is an additive Gaussian noise with variance σ_n^2, and $\mathbf{x}_p^{(n_t)}$ is the pilot sequence inserted in the n_t transmit antenna. In the following, using (11) we rewrite the $\mathbf{H}$ matrix in this form:

$$
\begin{bmatrix}
\tilde{\mathbf{H}}_{n_r,n_t}(I_{n_t}[1]) \\
\tilde{\mathbf{H}}_{n_r,n_t}(I_{n_t}[2]) \\
\vdots \\
\tilde{\mathbf{H}}_{n_r,n_t}(I_{n_t}[N_p])
\end{bmatrix}
= \mathrm{diag}(\tilde{\underline{H}}_{e,p})\mathbf{F}_{p,n_t}
\begin{bmatrix}
\mathbf{h}_{n_r,n_t}(0) \\
\mathbf{h}_{n_r,n_t}(1) \\
\vdots \\
\mathbf{h}_{n_r,n_t}(L-1)
\end{bmatrix}
\tag{14}
$$

where, $\tilde{\underline{H}}_{e,p}$ and $\mathbf{F}_{p,n_t}$ are respectively the selected shaping $1 \times N_p$ vector and the $N_p \times L$ corresponding Fourier transform matrix at I_{n_t} frequency index positions in the n_t transmit antenna :

$$
\mathbf{F}_{p,n_t} =
\begin{bmatrix}
w_{I_{n_t}[1]}^0 & w_{I_{n_t}[1]}^1 & \cdots & w_{I_{n_t}[1]}^{(L-1)} \\
w_{I_{n_t}[2]}^0 & w_{I_{n_t}[2]}^1 & \cdots & w_{I_{n_t}[2]}^{(L-1)} \\
\vdots & \vdots & \ddots & \vdots \\
w_{I_{n_t}[N_p]}^0 & w_{I_{n_t}[N_p]}^1 & \cdots & w_{I_{n_t}[N_p]}^{(L-1)}
\end{bmatrix}
\tag{15}
$$

$$
w_n^l = \exp(-2\pi j \frac{ln}{N})
$$

Finally, we can obtain this matrix form:

$$
\begin{bmatrix}
\tilde{\mathbf{Y}}_{n_r}(I_{n_t}[1]) \\
\tilde{\mathbf{Y}}_{n_r}(I_{n_t}[2]) \\
\vdots \\
\tilde{\mathbf{Y}}_{n_r}(I_{n_t}[N_p])
\end{bmatrix}
= \mathrm{diag}(\mathbf{x}_p^{(n_t)})\mathrm{diag}(\tilde{\underline{H}}_{e,p})\mathbf{F}_{p,n_t}\mathbf{h}_{n_r,n_t} +
\begin{bmatrix}
b_1 \\
b_2 \\
\vdots \\
b_{N_p}
\end{bmatrix}
\tag{16}
$$

Considering an Additive Gaussian Noise, the unbiased estimator of the channel impulse vector $\mathbf{h}_{n_r,n_t}$ according to the maximum likelihood criterion (ML) is exactly the one given by the unbiased least-square (LS) solution given by:

$$
\widehat{\mathbf{h}}_{n_r,n_t} = \left(\mathrm{diag}(\mathbf{x}_p^{(n_t)})\mathrm{diag}(\tilde{\underline{H}}_{e,p})\mathbf{F}_{p,n_t}\right)^+
\begin{bmatrix}
\tilde{\mathbf{Y}}_{n_r}(I_{n_t}[1]) \\
\tilde{\mathbf{Y}}_{n_r}(I_{n_t}[2]) \\
\vdots \\
\tilde{\mathbf{Y}}_{n_r}(I_{n_t}[N_p])
\end{bmatrix}
\tag{17}
$$

Using equation (11), the Frequency response is given by:

$$
\widehat{\mathbf{H}}_{n_r,n_t}(k) = \underline{H}_e(k) \sum_{l=0}^{L-1} \widehat{\mathbf{h}}_{n_r,n_t}(l)\ \exp(-2\pi j \frac{lk}{N})
\tag{18}
$$

$$
0 \leq k \leq N-1
$$

The previous equation can be written as:

$$
\widehat{\mathbf{H}}_{n_r,n_t} = \mathrm{diag}(\tilde{\underline{H}}_e)\mathbf{F}\ \widehat{\mathbf{h}}_{n_r,n_t}
\tag{19}
$$

where, $\mathbf{F}$ is the $N \times L$ corresponding Fourier transform matrix.

The corresponding Cramer-Rao bound (CRB) for this estimator can be evaluated in the following expressions:

$$
\begin{cases}
\mathrm{CRB}(\widehat{\mathbf{H}}_{n_r,n_t}) = \mathrm{diag}(\tilde{\underline{H}}_e)\mathbf{F}\ \mathrm{CRB}(\widehat{\mathbf{h}}_{n_r,n_t})\ \mathbf{F}^H \mathrm{diag}^H(\tilde{\underline{H}}_e) \\
\mathrm{CRB}(\widehat{\mathbf{h}}_{n_r,n_t}) = \sigma_n^2 \left\{\mathbf{V}^H \mathbf{V}\right\}^{-1}
\end{cases}
$$

where, $\mathbf{V} = \mathrm{diag}(\mathbf{x}_p^{(n_t)})\mathrm{diag}(\tilde{\underline{H}}_{e,p})\mathbf{F}_{p,n_t}$

The expression of the CRB for the impulse channel vector $\widehat{\mathbf{h}}_{n_r,n_t}$ is given by:

$$
\mathrm{CRB}(\widehat{\mathbf{h}}_{n_r,n_t}) = \frac{\sigma_n^2}{\sigma_p^2\ N_p} \mathbf{I}_{\mathbf{L,L}}
\tag{20}
$$

The expression of the CRB for the frequency response channel vector is deduced as follow:

$$
\mathrm{CRB}(\widehat{\mathbf{H}}_{n_r,n_t}) = \frac{L\ \sigma_n^2}{\sigma_p^2\ N_p} \mathrm{diag}(\underline{H}_e)\mathrm{diag}^H(\underline{H}_e)
\tag{21}
$$

The Mean Square Error of the estimator of $\widehat{\mathbf{H}}_{n_r,n_t}$ is the trace of the CRB matrix:

$$
\mathrm{MSE}\left(\widehat{\mathbf{H}}_{n_r,n_t}\right) = \frac{L\ \sigma_n^2}{\sigma_p^2\ N_p}\left(\frac{1}{N}\sum_{k=0}^{N}|\underline{H}_e(k)|^2\right)
$$

3) MMSE combining Equalization: In order to recover the data matrix sequence $\widehat{\mathbf{X}}^d = [\widehat{\mathbf{X}}_1^d, \widehat{\mathbf{X}}_2^d, \ldots, \widehat{\mathbf{X}}_{N_t}^d]^T$, among N columns, we estimate only K columns of $\mathbf{X}$ which correspond to the $\widehat{\mathbf{X}}^d$ matrix and having a frequency index $T_{cp} \leq k \leq N - T_{cp} - 1$. By exploiting the diversity of observation in the $\tilde{\mathbf{Y}}$ matrix given by the added cyclic prefix and cyclic suffix, a linear block MMSE combining equalization is considered:

$$
\begin{bmatrix}
\widehat{\mathbf{X}}_1(k) \\
\widehat{\mathbf{X}}_2(k) \\
\vdots \\
\widehat{\mathbf{X}}_{N_t}(k)
\end{bmatrix}
=
\begin{cases}
\mathbf{W}_1(k).[\mathbf{Y}(k) + \mathbf{Y}(k + (N - 2.T_{cp}))] \\
\quad T_{cp} \leq k \leq 2.T_{cp} - 1 \\
\mathbf{W}(k).\mathbf{Y}(k) \\
\quad 2.T_{cp} \leq k \leq N - 2.T_{cp} - 1 \\
\mathbf{W}_2(k).[\mathbf{Y}(k) + \mathbf{Y}(k - (N - 2.T_{cp}))] \\
\quad N - 2.T_{cp} \leq k \leq N - T_{cp} - 1
\end{cases}
\tag{22}
$$

$$
T_{cp} \leq k < N - T_{cp} \quad \text{and} \quad k \notin \{I_{n_t}\ ;\ \forall\ 1 \leq n_t \leq N_t\}
$$

Assuming γ is the signal-to-noise ratio (SNR) and,

$$
\begin{cases}
\mathbf{W}(k) = \mathbf{H}^H(k).\left(\mathbf{H}(k).\mathbf{H}^H(k) + \frac{N.\gamma^{-1}}{K}\mathbf{I}_{N_r}\right)^{-1} \\[2mm]
\mathbf{W}_1(k) = \mathbf{H}_1^H(k).\left(\mathbf{H}_1(k).\mathbf{H}_1^H(k) + \frac{N.\gamma^{-1}}{K}\mathbf{I}_{N_r}\right)^{-1} \\[2mm]
\mathbf{W}_2(k) = \mathbf{H}_2^H(k).\left(\mathbf{H}_2(k).\mathbf{H}_2^H(k) + \frac{N.\gamma^{-1}}{K}\mathbf{I}_{N_r}\right)^{-1}
\end{cases}
$$

where,

$$
\begin{cases}
\mathbf{H}_1(k) = \mathbf{H}(k) + \mathbf{H}(k + (N - 2.T_{cp})) \\
\mathbf{H}_2(k) = \mathbf{H}(k) + \mathbf{H}(k - (N - 2.T_{cp}))
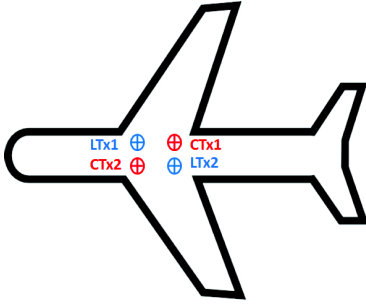\end{cases}
$$

Fig. 4. Position of Tx/Rx antennas in underside of the aircraft.

4) Time Domain: After equalization, we obtain an estimation of data symbols at each transmit antenna $\widehat{\mathbf{X}}^{\mathbf{d}} = [\widehat{\mathbf{X}}_1^{\mathbf{d}}, \widehat{\mathbf{X}}_2^{\mathbf{d}}, \ldots, \widehat{\mathbf{X}}_{N_t}^{\mathbf{d}}]^T$. Each row of this obtained matrix is transformed to the time domain by applying IFFT transformation to estimate the $\mathbf{C}$ matrix:

$$\widehat{\mathbf{C}}_{n_t}(k) = \sum_{m=0}^{K-1} \widehat{\mathbf{X}}_{n_t}^{\mathbf{d}}(m) \ \exp(2\pi j \frac{mk}{K}) \qquad (23)$$

$$1 \leq n_t \leq N_t \qquad 1 \leq m \leq K$$

5) Active antenna selection: For SM another source of information needs to be estimated at the receiver, namely, the spatial location (the selected antenna number) from which the symbol was transmitted. This is done by finding the location of the maximum of the absolute value of each column in the estimated matrix $\hat{\mathbf{C}}$ as follows:

$$\hat{a}_k = \max_{n_t} |\widehat{\mathbf{C}}_{n_t}(k)| \qquad 1 \leq k \leq K \qquad (24)$$

Then, the symbol detection is estimated by using the following equation:

$$\hat{c}_k = \mathbb{Q}(\hat{\mathbf{C}}_{\hat{a}_k}(k)) \qquad 1 \leq k \leq K \qquad (25)$$

where $\mathbb{Q}(.)$ is the constellation quantization (slicing) function.

III. APPLICATION : MISSION LINK OF AERONAUTICAL COMMUNICATIONS

One of the most promising avenues for achieving a constant and stable communication link is multi-antenna technology (MIMO). Multiple antennas allow the aircraft and Ground Stations to improve performance. Today the planes are able to communicate with ground stations in the two frequency bands allocated for UAS: in L-band from $960 - 977$ MHz and in C-band from $5030 - 5091$ MHz. For the mission link, signals will be transmitted via two antenna in the C-band CTX1 and CTx2 (respectively LTX1 and LTx2 in L-band). Fig.4 shows the location of the two receiver (Rx) antennas and the other two transmit antennas under the aircraft. The distance between L-band Rx1 and C-band Tx2 (or between C-band Rx1 and L band Tx2) antennas is $1.32 \ m$ [7]. Differently from control link where we have two main paths; a strong line-of-sight direct path LOS from satellite to aircraft and another scattering path result of ground reflections [8], in the mission link, we
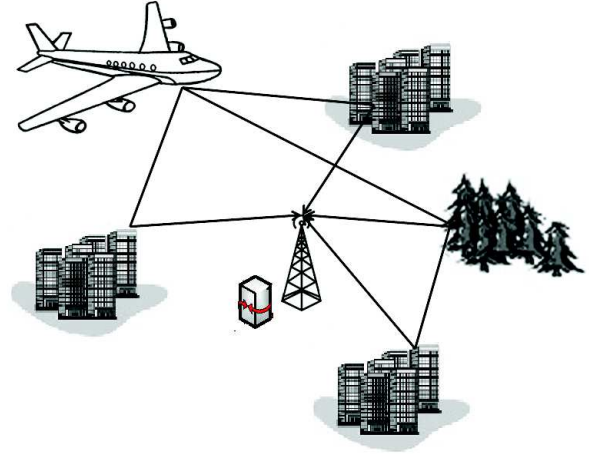

Fig. 5. Air-ground communications system.

have to deal with a multipath channel: The transmitted signal arrives at the receiver in various paths (see Fig.5) of different lengths and strengths.

A. Frequency channel fading

The Frequency fading is caused by the multipath signal propagation. This phenomenon happens because the environment in which the aircraft flies is composed of several obstacles, both natural and artificial, which are located randomly on the ground. Rivers, mountains and buildings are examples of elements that can alter the signal physical characteristics, imposing different attenuations and phase changes. This random features of the environment makes it necessary to model the channel using a statistical approach. Over time a large number of distributions were proposed for various specifics cases. Indeed, without a line-of-sight (LOS), the frequency channel gain can be modeled by a Rayleigh process [9]. The environment has a feature that is the aircraft most of the time has a line-of-sight (LOS) with the ground station with which it communicates. This allows the frequency channel gain $\rho = |\tilde{\mathbf{H}}_{n_r,n_t}(k)|$, in this case, to be modeled by the Rice probability distribution [9] expressed by:

$$f(\rho) = \frac{\rho}{\sigma^2} \exp(\frac{-(\rho^2 + A_{LOS}^2)}{2 \ \sigma^2}) I_0(\frac{A_{LOS} \cdot \rho}{\sigma^2}) \qquad (26)$$

where $I_0(.)$ is the modified Bessel function of order 0, A_{LOS} is the amplitude of the direct component and σ is the power of the diffuse components given as:

$$\sigma^2 = \sum_{l=1}^{L} P_{\text{rms}}(l) \qquad (27)$$

where $P_{\text{rms}}(l)$ is the effective (or rms) power of the lth scattered path and L is the number of paths.

The Rice distribution has a parameter that determines the relationship between the powers of the direct and diffuse components of the signal, which is defined as:

$$K_{LOS} = \frac{A_{LOS}^2}{\sigma^2} \qquad (28)$$

particularly, in some environments, the direct component is absent. For example, for an urban environment and lower altitude, there is no visual line-of-sight (LOS) between the transmitting antenna and the receiving antenna ($A_{LOS} = 0$) [9]. In this context Non-line-of-sight (NLOS) multipath channel is considered.

B. Delay

A simple geometrical analysis reveals that $\Delta d \approx h$ [10] for air-ground links, if one dominant reflector is present, where h is the altitude of the aircraft. This geometrical analysis is based on the fact that during the flight, the aircraft distance to the base station is large compared to its altitude, so that the projected distance on the ground is about the same as the real distance. If now reflection, scattering, or diffraction occurs on objects on the ground, the maximum detour distance can be estimated to be the aircraft altitude for air-ground communication:

$$\tau_{\max} = \frac{\Delta d}{3 10^8} \approx \frac{h}{3 10^8} \qquad (29)$$

Assuming a typical maximum altitude of $2100m$ [11], one obtains $\tau_{\max} = 7\mu s$.

C. Doppler

The scenario is characterized by fast fading: $v = 25..40\ m/s$ [10]. During the arrival of the base station, the scattered components are typically not isotropically distributed, i.e., the beamwidth of the scattered components $\Lambda = \varphi_{aH} - \varphi_{aL}$ is less than 360° [10] (see Fig.6). φ_{aL} is the lowest angle and φ_{aH} is the highest angle of arrival signals from the aircraft antenna to the ground base station antenna. In [12], a beamwidth of $\Lambda \leq 360°$ was considered and a corresponding Doppler spectrum was derived, assuming that the scatterers are uniformly distributed within the beamwidth. This non-isotropical distribution results in a Doppler probability density function $P(f)$, that is only a part of the classical 2-D isotropic Doppler density function derived by Clarke [13] [14] distribution:

$$P(f) = \frac{1}{\Lambda \cdot f_{\max} \sqrt{1 - (\frac{f}{f_{\max}})^2}} \qquad (30)$$

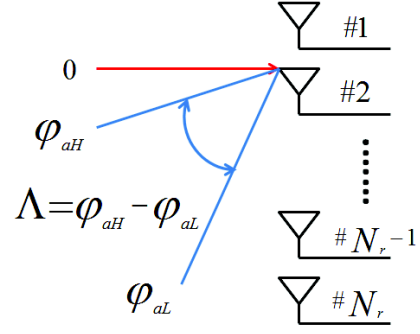$$f_{\max} \cos(\varphi_{aL}) \leq f \leq f_{\max} \cos(\varphi_{aH})$$

Fig. 6. Beamwidth of the received signals.

IV. SIMULATION RESULTS

The performance analysis is proposed for SISO, SIMO and SM-MIMO system. The BER performance were determined using a Monte Carlo simulation. Each simulation was conducted over 500 data frames. The frequency used in the simulator was 5 GHz ($\lambda = 0.06\ m$) and the bandwidth was set to 10 MHz ($Ts = 0.2\ \mu s$). Each Frame contain $K = 378$ symbols to be transformed to the frequency domain and extended to $N = 512\ (0.5\ k)$ before pre-shaped by $\underline{H}_e(n)$ with a roll-off $\beta = 0.25$. For channel estimation we will use a CAZAC sequence of length $N_p = 23$ to be injected in each transmit antenna $n_t \in \{1, 2\}$. For the receiver we consider $N_r \in \{1, 2, 3, 4\}$ receive antennas.

A. PAPR comparison

SS SC-OFDM offers similar performance and complexity as SC-OFDM , SC-CP and OFDM. However, the main advantage of SS SC-OFDM is the low PAPR (peak-average-power ratio) of the transmit signal. PAPR is defined as the ratio of the peak power to average power of the transmit signal. PAPR
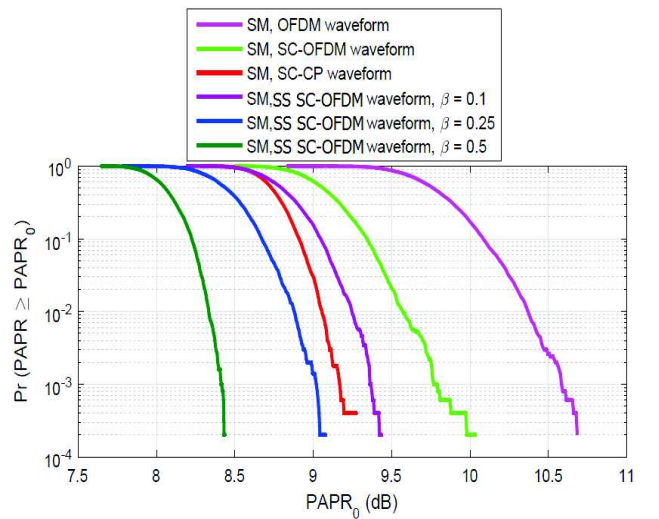

Fig. 7. PAPR for each β choice

comparison between SS SC-OFDM, SC-CP, SC-OFDM and OFDM variations has been done in Fig.8. With pulse shaping filter, SS SC-OFDM shows the best PAPR. Compared to OFDM PAPR, in SM Modulation, the PAPR of SS SC-OFDM with roll-off $\beta = 0.5$ with QPSK is about 2 dB lower, whereas that with $\beta = 0.1$ is only about 1 dB lower. Therefore, SS SC-OFDM is a preferred modulation technique for lower PAPR.

B. Channel estimation gain

The Frequency channel estimation performance is shown in Fig.8. The red curve represents the Mean Square Error (MSE) of the estimation using the reduced-rank (rr) LS channel estimation technique presented in Section II-C2. The blue curve represents the result using the linear interpolation technique. This simulation shows that the reduced rank estimator gives an important gain compared to interpolation method and reaches the Cramer-Rao bound.
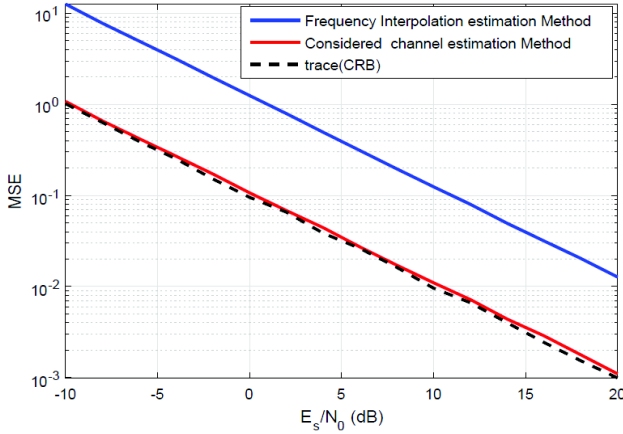

Fig. 8. MSE, CRB for the frequency aeronautical channel estimation.

C. Spatial demodulation

The BER performance in Fig.9, Fig.10 and Fig.11 perform the comparison of SM and SIMO system for the same spectral efficiency set to 3-b/s/Hz considering Rayleigh channel ($K_{LOS} = -\infty$) and two Rice channels with respectively $K_{LOS} = -1$ dB and $K_{LOS} = 4.25$ dB. The results show that performance increases with the number of receive antennas.

1) Low elongation / Low altitude scenario: For this scenario we consider two environments; the urban environment and the mountainous environment.

Urban environment: In urban environment for low elongation/low altitude case, Fig.9 shows the BER performance for NLOS channel model. In SISO case, we see that performances are very affected by the channel. Thus, the introduction of SM technique is here to address this issue. In multi-antenna system the performance is determined by the spread of the signal in space, in addition to the noise and the delay spread seen in the SISO case. In NLOS channel model, the matrix $\mathbf{H}_{n_r,n_t}(k)$ has a full rank, that's why we have interest to lead multi-antenna techniques. In this simulation, results show that we obtained
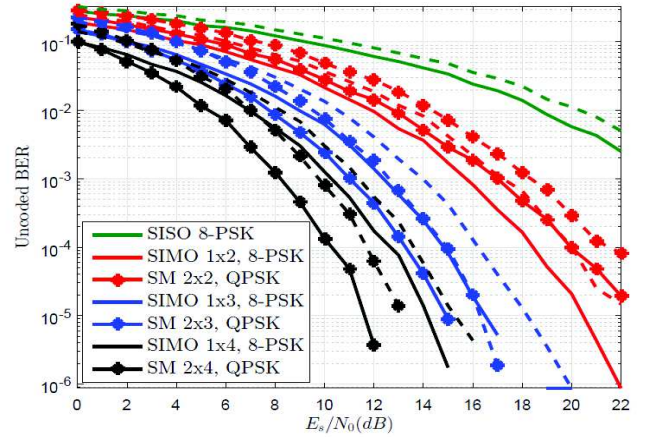

Fig. 9. BER performance in urban environment for low elongation/low altitude scenario; dashed curves represent the performance with channel estimation and solid curves present the case with perfect channel estimation.

a gain of 2 dB in the resulting use of $N_r = 4$ receive antennas compared to the SIMO case with the same receive antennas number. For $N_r = 2$ the gain is about 1 dB. However, for $N_r = 2$, SIMO performance are slightly better.

Mountainous environment: Similar to the coastal environment and the flat desert environment, in mountainous environment, the aeronautical channel can be modeled by a Rice process. In this case, we assume $K_{LOS} = -1$ dB.

Fig.10 show that with the use of $N_r = 4$ receive antennas, the BER performance in SM 2×4 modulation is slightly better than the considered SIMO 1×4 case. For $N_r = 3$ and $N_r = 2$, SIMO performance better than SM-MIMO performance.
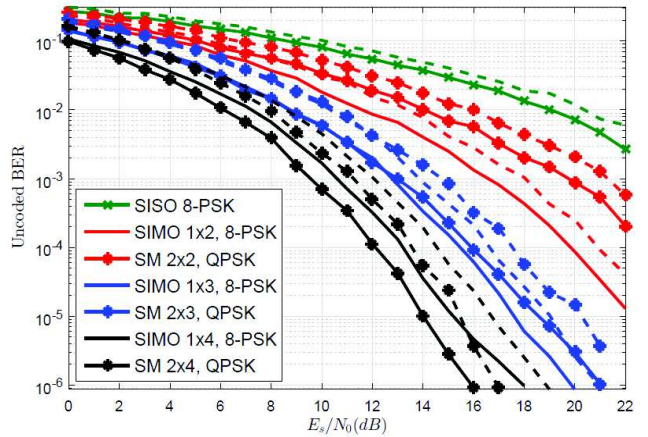

Fig. 10. BER performance in mountainous environment for low elongation/low altitude scenario; dashed curves represent the performance with channel estimation and solid curves present the case with perfect channel estimation.

2) high elongation / median altitude scenario: In this scenario and for most environments, the aeronautical channel is modeled by a Rice process with a Rice factor K_{LOS} depending of the nature of the each environment.

Fig.11 performs the scenario with high elongation/median altitude in urban environment. In this simulation we consider, we consider $K_{\text{LOS}} = 4,25$ dB (urban environment). In this case we present a important correlation between the received signals because the considerable presence of the deterministic LOS component. Thus the diversity gain is lower and the SIMO performance are better than the SM performance.
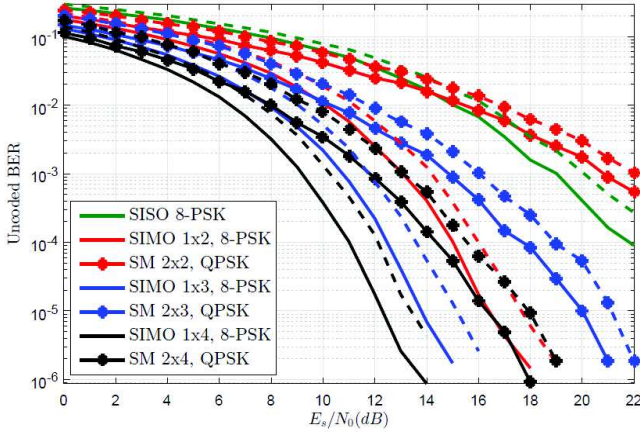

Fig. 11. BER performance in urban environment for high elongation/median altitude scenario; dashed curves represent the performance with channel estimation and solid curves present the case with perfect channel estimation.

To conclude, spatial modulation technique can be applied for NLOS scenario or for low K_{LOS} levels cases. Otherwise, there will be no gain in performance compared to the SIMO configuration.

V. CONCLUSION

In this paper, we proposed a SM-MIMO transmission scheme to improve the spectral efficiency. In the scheme, we conducted SS SC-OFDM waveform to reduce PAPR. we detailed the different parts of receiver and the various associated algorithms. Then, we have considered the aeronautical communications case by including the model of aeronautical channel for the NLOS and the LOS scenario.

Depending on the value of K_{LOS}, the SM technique can realize a considerable gain compared to the SIMO configuration. In fact, for low values of K_{LOS}, SM provides a better performance in terms of BER.

SS SC-OFDM waveform aims to limit the problem of non-linearity at the receiver. Future works will investigate the effect of non-linearity and digital predistortion data associated methods to reduce the non-linearity impact at the receiver.

ACKNOWLEDGMENT

REFERENCES

[1] A. M. Samad, N. Kamarulzaman, M. A. Hamdani, T. A. Mastor, and K. A. Hashim, "The potential of unmanned aerial vehicle (uav) for civilian and mapping application," in *System Engineering and Technology (ICSET), 2013 IEEE 3rd International Conference on*, Aug 2013, pp. 313–318.

[2] M. D. Renzo, H. Haas, and P. M. Grant, "Spatial modulation for multiple-antenna wireless systems: a survey," *IEEE Communications Magazine*, vol. 49, no. 12, pp. 182–191, December 2011.

[3] R. Mesleh, H. Haas, C. W. Ahn, and S. Yun, "Spatial modulation - a new low complexity spectral efficiency enhancing technique," in *2006 First International Conference on Communications and Networking in China*, Oct 2006, pp. 1–5.

[4] R. Y. Mesleh, H. Haas, S. Sinanovic, C. W. Ahn, and S. Yun, "Spatial modulation," *IEEE Transactions on Vehicular Technology*, vol. 57, no. 4, pp. 2228–2241, July 2008.

[5] B. Ros, S. Cazalens, C. Boustie, and X. Fouchet, "SC-FDMA Waveform Enabling Frequency Holes in a Shared Spectrum Context," *IARIA SPACOMM 2015: The Seventh International Conference on Advances in Satellite and Space Communications, Barcelona, Spain*, pp. 1–6, 2015.

[6] B. Benammar, N. Thomas, M. L. Boucheret, C. Poulliat, and M. Dervin, "Analytical expressions of power spectral density for general spectrally shaped sc-fdma systems," in *21st European Signal Processing Conference (EUSIPCO 2013)*, Sept 2013, pp. 1–5.

[7] D. W. Matolak, "Unmanned aerial vehicles: Communications challenges and future aerial networking," in *Computing, Networking and Communications (ICNC), 2015 International Conference on*, Feb 2015, pp. 567–572.

[8] B. Raddadi, C. Poulliat, N. Thomas, M. L. Boucheret, and B. Gadat, "Channel estimation with a priori position for aeronautical communications via a satellite link," in *Personal, Indoor, and Mobile Radio Communications (PIMRC), 2015 IEEE 26th Annual International Symposium on*, Aug 2015, pp. 532–537.

[9] D. W. Matolak, "Air-ground channels amp; models: Comprehensive review and considerations for unmanned aircraft systems," in *Aerospace Conference, 2012 IEEE*, March 2012, pp. 1–17.

[10] E. Haas, "Aeronautical channel modeling," *IEEE Transactions on Vehicular Technology*, vol. 51, no. 2, pp. 254–264, Mar 2002.

[11] S. Blandino, F. Kaltenberger, and M. Feilen, "Wireless channel simulator testbed for airborne receivers," in *2015 IEEE Globecom Workshops (GC Wkshps)*, Dec 2015, pp. 1–6.

[12] S. M. Elnoubi, "A simplified stochastic model for the aeronautical mobile radio channel," in *Vehicular Technology Conference, 1992, IEEE 42nd*, May 1992, pp. 960–963 vol.2.

[13] R. H. Clarke, "A statistical theory of mobile-radio reception," *The Bell System Technical Journal*, vol. 47, no. 6, pp. 957–1000, July 1968.

[14] M. J. Gans, "A power-spectral theory of propagation in the mobile-radio environment," *IEEE Transactions on Vehicular Technology*, vol. 21, no. 1, pp. 27–38, Feb 1972.